Acta Oceanol. Sin., 2020, Vol. 39, No. 1, P. 91–101
https://doi.org/10.1007/s13131-019-1522-3
http://www.hyxb.org.cn
E-mail: hyxbe@263.net

Validation of MODIS ocean-colour products in the coastal waters of the Yellow Sea and East China Sea

Lingling Jiang[1]*, Xiangyu Guo[1], Lin Wang[2], Shubha Sathyendranath[3], Hayley Evers-King[3], Yanlong Chen[2], Bingnan Li[2]

[1] College of Environmental Science and Engineering, Dalian Maritime University, Dalian 116026, China

[2] Ministry of Ecology Environment, National Marine Environmental Monitoring Center, Dalian 116023, China

[3] Plymouth Marine Laboratory (PML), Plymouth, Devon , PL1 3DH, UK

Received 29 December 2018; accepted 5 May 2019

Abstract

An extensive study collected in situ data along the Yellow Sea (YS) and East China Sea (ECS) to assess the radiometric properties and the concentration of the water constituents derived from Moderate Resolution Imaging Spectroradiometer (MODIS). Thirteen high quality match-ups were obtained for evaluating the MODIS estimates of $R_{rs}(\lambda)$, chlorophyll *a* (Chl *a*) and concentrations of suspended particulate sediment matter (SPM). For MODIS $R_{rs}(\lambda)$, the mean absolute percentage difference (APD) was in the range of 20%–36%, and the highest uncertainty appeared at 412 nm, whereas the band ratio of $R_{rs}(\lambda)$ at 488 nm compared with that at 547 nm was highly consistent, with an APD of 7%. A combination of near-infrared bands and shortwave infrared wavelengths atmosphere correction algorithm (NIR-SWIR algorithm) was applied to the MODIS data, and the estimation accuracy of R_{rs} were improved at most of the visible spectral bands except 645 nm, 667 nm and 678 nm. Two ocean-colour empirical algorithms for Chl *a* estimation were applied to the processed data, the results indicated that the accuracy of the derived Chl *a* values was obviously improved, the four-band algorithms outperformed the other algorithm for measured and simulated datasets, and the minimum APD was 35%. The SPM was also quantified. Two regional and two coastal SPM algorithms were modified according to the in situ data. By comparison, the modified Tassan model had a higher accuracy for the application along the YS and ECS with an APD of 21%. However, given the limited match-up dataset and the potential influence of the aerosol properties on atmosphere correction, further research is required to develop additional algorithms especially for the low Chl *a* coastal water.

Key words: MODIS, turbid waters, chlorophyll a, SPM, retrieval algorithms, Yellow and East China Sea

Citation: Jiang Lingling, Guo Xiangyu, Wang Lin, Sathyendranath Shubha, Evers-King Hayley, Chen Yanlong, Li Bingnan. 2020. Validation of MODIS ocean-colour products in the coastal waters of the Yellow Sea and East China Sea. Acta Oceanologica Sinica, 39(1): 91–101, doi: 10.1007/s13131-019-1522-3

1 Introduction

Satellite ocean-colour remote sensing plays an important role in providing critical ocean information on global, regional and local scales. Typical ocean-colour sensors such as Sea-viewing Wide Field-of-view Sensor (SeaWiFS), Moderate Resolution Imaging Spectroradiometer (MODIS) and Medium Resolution Imaging Spectrometer (MERIS) provide high acquisition frequency bands ideally positioned for the detection of water constituents and primary production estimation.

In coastal waters, chlorophyll *a* (Chl *a*) is a good indicator of primary productivity and suspended particulate matter (SPM) can affect the light transmission in water. As key indicators of water quality, remote sensing estimations of these two parameters have achieved many results (Gitelson et al., 2007; Kuchinke et al., 2009; Han et al., 1994; Shen et al., 2010; Cheng et al., 2013). However, some of these satellite Chl *a* and SPM algorithms tend to fail in case II water due to the optical complexity and overlapping and uncorrelated absorptions by the coloured dissolved organic material (CDOM) and the non-algal particles (Moses et al., 2009; Carder et al., 2004; Darecki and Stramski, 2004). Although the accuracy of Chl *a* and SPM algorithms for some satellite sensors in certain coastal zones has already been evaluated (Zibordi et al., 2006; Cui et al., 2010), calibration and validation of the various products in different coastal ocean regions are still important for ocean colour missions.

The MODIS onboard the Aqua satellite (MODIS-Aqua), launched in May 2002, is the current operational, medium resolution mission from NASA. There have been few previous MODIS validation studies in coastal waters (Zibordi et al., 2009; Dall'Olmo et al., 2005; Menon et al., 2006; Tilstone et al., 2013; Gitelson et al., 2008), and MODIS has recently experienced radiometric drift, which has been addressed through frequent vicarious calibration and re-processing of the data (Tilstone et al., 2013; Xiao et al., 2018). But few for the SPM and Chl *a* products are available from MODIS-Aqua in the YS and ECS (Bian et al., 2013; Zhang et al., 2010; Sun et al., 2010). Therefore, it is necessary to assess the

Foundation item: The National Natural Science Foundation of China under contract Nos 41506197 and 41406199; the Doctoral Scientific Research Foundation of Liaoning Province under contract No. 201501190; the Fundamental Research Funds for the Central Universities under contract No. 3132017110.

*Corresponding author, E-mail: jiangll@dlmu.edu.cn

MODIS-Aqua algorithms in these coastal areas to identify the most accurate Chl *a* and SPM products available for the region in terms of on-going monitoring of phytoplankton biomass.

The principle objective of this study is to assess the performance of the major MODIS-Aqua products in the turbid water along the East China Coast on in-situ measurements and match-up analysis, including $R_{rs}(\lambda)$, SPM and Chl *a*. The effects of potential errors in the atmospheric correction were assessed. Subsequently, the ocean-colour algorithms and spatial-temporal match-up differences were analyzed.

2 Data and methodology

2.1 *Study area*

The water mass in the Yellow Sea (YS) and Eest China Sea (ECS) regions is considered typical case II water (Li et al., 2017). The YS and ECS are located within the marginal sea of the northwest Pacific Ocean. This semi-enclosed, wide shelf sea consists of complicated hydrological variations and high sediment concentrations, with clear seasonal changes over a wide region (Fig. 1).

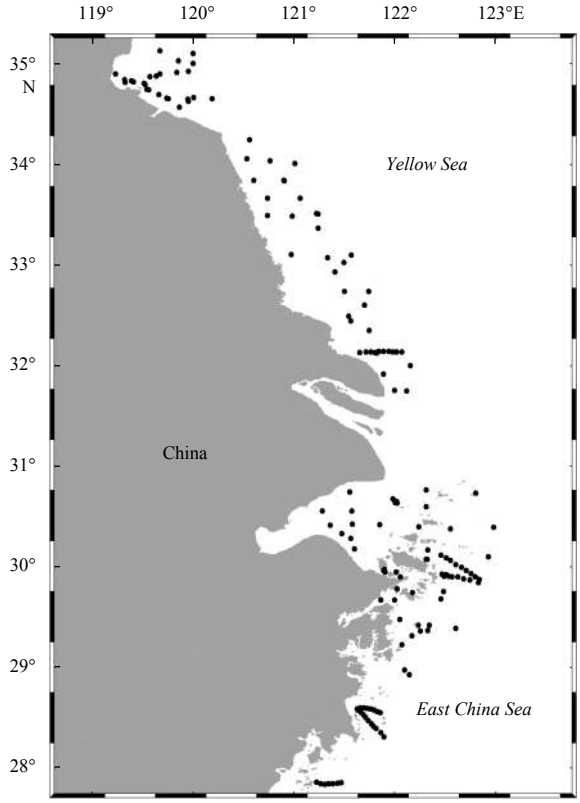

Fig. 1. Stations sampled along the Yellow Sea and East China Sea.

The YS is mainly contaminated by industrial pollution, agricultural runoff, and domestic sewage. The ECS is a marginal sea off the east coast of China. The Changjiang (Yangtze River) is the largest river flowing into the ECS and exports abundant nutrients and large amounts of sediments to the estuary (Gao and Song, 2005). Therefore, the coastal water near the estuary is well known for its extremely high turbidity (Zhang et al., 2010).

2.2 *In-situ data*

The *in-situ* dataset in this study contained 156 SPM, $R_{rs}(\lambda)$ and Chl *a* measurements that were collected from May 2012 to May 2014 during eight separate cruises (Fig. 1). Water-leaving $R_{rs}(\lambda)$ was measured with a hand-held ASD (Analyti-cal Spectral Device, Inc.) spectrometer following the NASA Ocean Optics protocols (Mueller et al., 2003). The "above-water method" is preferred to determine the value. This specific method was similar to the one utilized by Wang et al. (2012), in which R_{rs} was calculated from the following formula:

$$R_{rs} = \frac{L_w(\lambda, 0^+)}{E_d(\lambda, 0^+)} = \frac{L_{sfc}(\lambda, 0^+) - \rho L_{sky}(\lambda, 0^+)}{E_d(\lambda, 0^+)}, \quad (1)$$

where $L_w(\lambda, 0^+)$ is the water leaving radiance (W/(m²·nm·sr)); $E_d(\lambda, 0^+)$ is the above surface downwelling spectral irradiance (W/(m²·nm)); $L_{sfc}(\lambda, 0^+)$ is the above-water upwelling radiance; $L_{sky}(\lambda, 0^+)$ is the sky diffuse radiance; and ρ is the dimensionless air-water reflectance, which is always in the range of 0.022–0.05 (Lee et al., 1996; Tang et al., 2004) and was set at 0.028 for this study (Mobley, 1999). Among the curves obtained by the measurement, we selected data between 400 nm and 900 nm to calculate the remote sensing reflectance. The median repeated measurement was selected, and the remote sensing reflectance was resampled to 1 nm intervals. The $R_{rs}(\lambda)$ spectra (Fig. 2) depicts typical turbid coastal water, with large variability in magnitude, a roughly similar shape, and dominant peaks near 580 nm. Meanwhile, some high values around 700 nm are attributed to the scattering of suspended material.

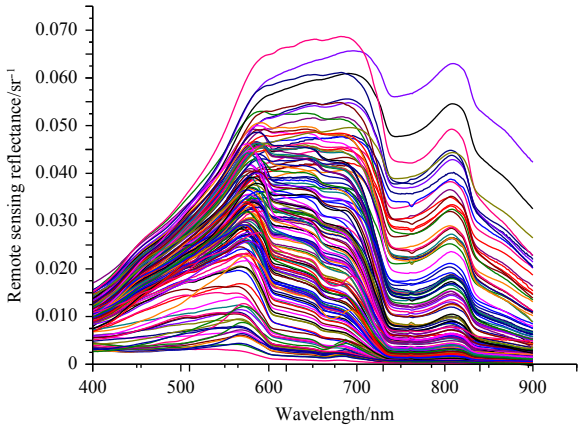

Fig. 2. Remote sensing reflectance $R_{rs}(\lambda)$ spectra at major ocean-colour bands.

SPM concentration was measured by the weighing method, where the water sample was filtered through a 0.45 μm vacuum filtration system. The filter pad was flushed with 50 cm³ of distilled water 3 times to remove the salt. The dry-weight of the filter-pad was weighed by an electronic analytic scale with 0.01 g/m³. The blank filter and sampled filter-pad were scaled several times, and two successive weight readings were within 0.01 g/m³ (Tang et al., 2004). We found that the SPM of the study area was in the range of 1.33 g/m³ and 958 g/m³. The histogram of SPM measurements is shown in Fig. 3 and indicates that the typical SPM value for this study area is less than 50 g/m³.

The Chl *a* concentration was determined by a fluorometric method (Cui et al., 2010), where the water samples were filtered through Whatman GF/F glass microfibre filters under a vacuum of less than 5×10^4 Pa. The volumes of the water samples were 200 mL for the mesotrophic area and 300–500 mL for the relatively clear area. The filters were analyzed immediately with a TD-700 fluorometer. Chl *a* concentration varied from 0.129 mg/m³ to

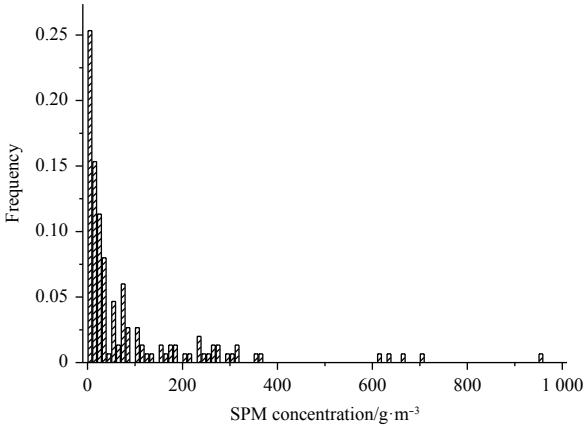

Fig. 3. Histogram of *in-situ* SPM concentration.

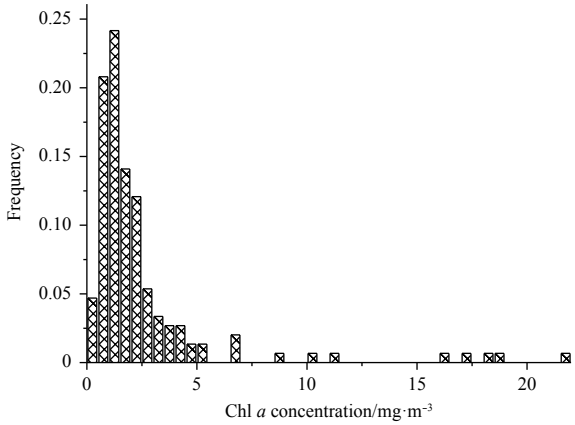

Fig. 4. Histogram of *in-situ* Chl *a* concentration.

21.6 mg/m³ (Fig. 4), with the typical Chl *a* concentration less than 5.25 mg/m³. Analysis of the replicate measurements gave an average difference of about ±10%.

2.3 *Match-up analysis*

MODIS-Aqua level-2 data, corresponding to the days of in situ sampling, were obtained from the NASA Ocean Biology Processing Group where the spatial resolution is approximately 1 km by 1 km (http://oceandata.sci.gsfc.nasa.gov). The data included remote sensing reflectance R_{rs} at bands of 412, 443, 469, 488, 531, 547, 555, 645, 667 and 678 nm, Chl *a* (by OC3M algorithm), aerosol optical thickness at band 869 nm and K_d (490).

Of the *in-situ* dataset, a total of 13 match-ups were obtained. These were extracted by a 3×3 pixel box around the sampled station, within ±3 h of sampling. The match-up dataset was established according to the procedure used by Cui et al. (2010). The dates of the MODIS image satisfying the match-up criteria are July 29, 2012; October 18, 2012 and May 26, 2014. The spatial distribution of the match-ups are shown in Fig. 5.

To evaluate the algorithm performance, we used the average of the absolute percentage difference (APD), average of relative percentage difference (RPD), root mean square error (RMS), median and semi-interquartile range of satellite to *in-situ* ratios (Ratio, SIQR) (Bailey et al., 2006). These quantities were calculated as follows:

$$APD = \frac{1}{N}\sum_{i=1}^{N}\frac{|y_i - x_i|}{x_i} \times 100\%, \tag{2}$$

$$RPD = \frac{1}{N}\sum_{i=1}^{N}\frac{y_i - x_i}{x_i} \times 100\%, \tag{3}$$

$$RMS = \sqrt{\frac{\sum_{i=1}^{N}(y_i - x_i)^2}{N}}, \tag{4}$$

$$SIQR = \frac{(Q_3 - Q_1)}{2}, \tag{5}$$

where x_i is the *in situ* value, y_i is the satellite-retrieved value, N is the number of match-up data points. Q_1 and Q_3 are the first and third quartiles, respectively. All the statistics were calculated using a linear scale.

3 Results

3.1 *R_{rs} assessment*

Table 1 shows the comparison results between MODIS $R_{rs}(\lambda)$

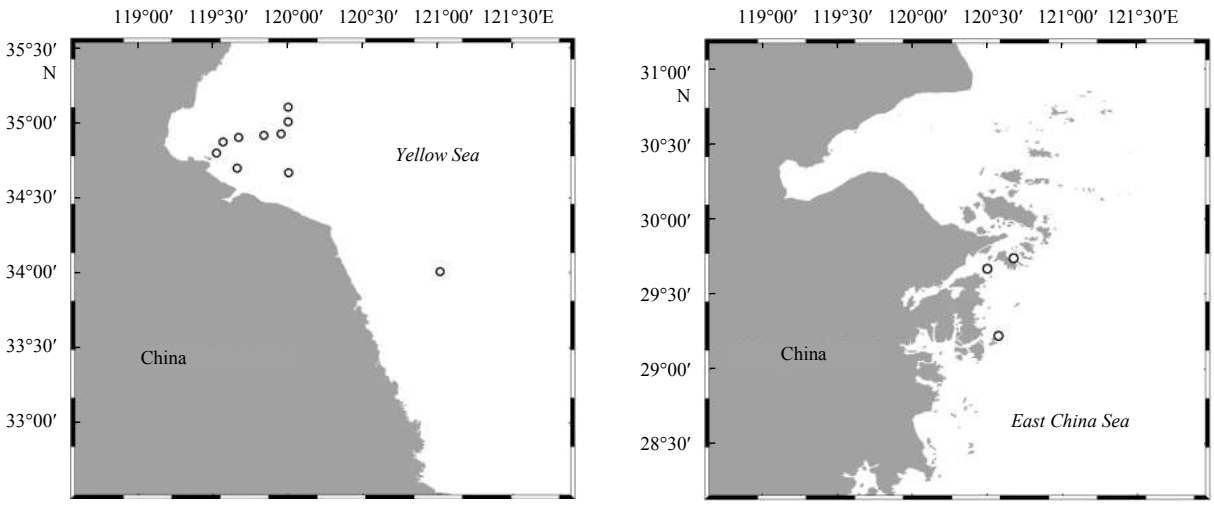

Fig. 5. Maps of the valid match-ups datasets for MODIS.

Table 1. Statistical results for the satellite-derived radiometric products evaluation

$R_{rs}(\lambda)$	APD/%	RMS	RPD/%	Ratio	SIQR	R^2	Slope	Intercept
$R_{rs}(412)/sr^{-1}$	36	0.003 0	–30	0.859	0.292	0.796	1.190	–0.003 6
$R_{rs}(443)/sr^{-1}$	23	0.002 7	–16	0.862	0.154	0.836	0.953	–0.001 0
$R_{rs}(469)/sr^{-1}$	22	0.003 1	–15	0.840	0.151	0.836	0.887	–0.000 4
$R_{rs}(488)/sr^{-1}$	22	0.003 7	–15	0.810	0.275	0.826	0.802	0.000 7
$R_{rs}(531)/sr^{-1}$	20	0.004 4	–11	0.827	0.099	0.844	0.749	0.002 3
$R_{rs}(547)/sr^{-1}$	20	0.005 0	–12	0.788	0.085	0.855	0.726	0.002 7
$R_{rs}(555)/sr^{-1}$	23	0.006 2	–17	0.754	0.084	0.859	0.671	0.002 8
$R_{rs}(645)/sr^{-1}$	30	0.009 0	–16	0.783	0.059	0.739	0.467	0.003 6
$R_{rs}(667)/sr^{-1}$	30	0.009 2	–15	0.793	0.056	0.653	0.408	0.003 8
$R_{rs}(678)/sr^{-1}$	30	0.009 3	–17	0.791	0.057	0.631	0.392	0.003 8
$R_{rs}(555)+R_{rs}(645)/sr^{-1}$	26	0.014	–18	0.083	0.754	0.830	0.572	0.007
$R_{rs}(555)+R_{rs}(667)/sr^{-1}$	26	0.015	–17	0.751	0.088	0.803	0.549	0.007 4
$R_{rs}(488)/R_{rs}(555)$	8	0.073	2	1.007	0.062	0.003	0.020	0.746 4
$R_{rs}(555)/R_{rs}(667)$	17	0.423	6	0.983	0.063	0.894	0.842	0.387 6
$R_{rs}(443)/R_{rs}(555)$	17	0.121	1	1.039	0.134	0.307	–1.041	1.114 3
$R_{rs}(412)/R_{rs}(488)$	30	0.252	–21	0.892	0.288	0.020	–0.563	0.771 6
$R_{rs}(443)/R_{rs}(547)$	15	0.119 0	–6	0.978 7	0.117 4	0.168 6	–0.935 4	1.052 7
$R_{rs}(488)/R_{rs}(547)$	7	0.075 6	–4	0.946 6	0.048 0	0.075 1	–0.133 3	0.838 1

and *in-situ* $R_{rs}(\lambda)$, while the scatter plots are shown in Fig. 6. The APD for the individual bands ranged from 20% to 36%, the lowest uncertainties appeared at 531 nm and 547 nm, and the highest APD was at 412 nm. For the band combination, $R_{rs}(488)/R_{rs}(547)$ and $R_{rs}(488)/R_{rs}(555)$ yield a lower uncertainties with an APD of 7% and 8%, respectively. $R_{rs}(555)/R_{rs}(667)$ and $R_{rs}(443)/R_{rs}(555)$ also have better accuracy, both with an APD of 17%. The ratio (<1) and the RPD (<0) indicated that the MODIS $R_{rs}(\lambda)$ underestimated the *in-situ* measurements at all visible bands. This underestimation is more pronounced at 412 nm. The coefficient of determination R^2 was lower in the red bands than that in the green and blue bands, and the slope was 0.953 for $R_{rs}(443)$ and 0.887 for $R_{rs}(469)$, but 0.408 and 0.392 for $R_{rs}(667)$ and $R_{rs}(678)$, respectively. For the band combination, $R_{rs}(488)/R_{rs}(547)$ and $R_{rs}(488)/R_{rs}(555)$ have a better performance with an APD of 7% and 8%, and $R_{rs}(455)/R_{rs}(667)$ and $R_{rs}(443)/R_{rs}(555)$ also have higher accuracy, both with an APD of 17%.

Figure 7 shows the comparison between the *in-situ* measurements and satellite retrievals for the 13 match-ups, indicating high levels of agreement at the majority of stations.

3.2 *SPM and Chl a concentration assessment*

The results of Chl *a* from MODIS products are shown in Table 2 as well as Fig. 10a. The derived Chl *a* value overestimated the *in-situ* ones, with the ratios of MODIS values to those of *in-situ* values being 2.72. Uncertainties in the satellite Chl *a* were 132% and 2.49 in RMS, and the determination coefficient was 0.05, with a slope of 0.007 6.

There is no standard MODIS SPM product. To identify the source of the uncertainty, two regional SPM retrieval algorithms for the YS and ECS were evaluated and modified according to our in situ data. One is the Tang model (Tang et al., 2004), which utilizes the reflectance at bands of 488, 555, and 667 nm. The other is the Zhang model (Zhang et al., 2010), which utilizes the reflectance at bands of 488, 555, and 645 nm. From Table 3 and Fig. 8, it is obvious that the performance of the adjusted models are better than the original ones. Therefore, the modified model were applied to the MODIS data. The APDs were 49% and 33%, respectively (Table 2). The average relative error between the inversed SPM when using the Tang model and the measured SPM was higher than the results of Cui et al. (2014a). And we obtained a higher APD than that of Zhang et al. (2010) (26%). The retrieval accuracy of the SPM was significantly better than that of Chl *a* for the MODIS data, but the improved model is still needed for this region.

4 Discussion

4.1 *Atmospheric correction*

Compared with $R_{rs}(\lambda)$ validation results in the study area, it is noted that Cui et al. (2014) and Sun et al. (2010) obtained similar results, with RMS values of 0.002 4–0.003 9 sr^{-1} and 0.002 4–0.003 6 sr^{-1}, and APDs of 18%–28% and 21%–40%, respectively. While the RMS range is slightly larger in our study, in the range between 0.002 7 sr^{-1} and 0.009 3 sr^{-1}. In addition, the largest uncertainty occurred at the blue band 412 nm and the satellite $R_{rs}(\lambda)$ were underestimated, whereas we found the values were overestimated at this band in Cui's study, which may be attributed to the spatial distribution of the match-ups, the sediment-dominated water, and/or the elevated turbidity, which triggers many bio-optical models within the atmospheric correction process and accounts for non-negligible near-infrared $R_{rs}(\lambda)$ (Bailey et al., 2010). The short wave infrared method (SWIR) was used for the East China Sea, Zhang et al. (2010) found that this algorithm is also invalid in highly turbid waters. Wang and Shi (2007) proposed a combination of the near-infrared bands (NIR) algorithm and SWIR algorithm (NIR-SWIR algorithm) that can effectively remove the atmospheric contribution over highly turbid coastal and clear waters (Wang et al., 2009).

Thus, the NIR-SWIR method has been applied to our data. The results were shown in Table 5 for the comparison between in situ and inversion R_{rs}. It is clearly that the estimation accuracy of R_{rs} was improved at most of the visible spectral bands except 645, 667 and 678 nm. That is still a legitimate question (Chen et al., 2015). High turbidity levels may cause non-negligible $R_{rs}(1\,240)$ so that atmosphere correction using SWIR bands may be wrong from the beginning to the subsequent extrapolation (Knaeps et al., 2012; Shi and Wang, 2014; Doxaran et al., 2006). Furthermore, SWIR bands have lower signals-to-noise ratio (SNR) than the NIR, which often makes processed products to be poor (Van-

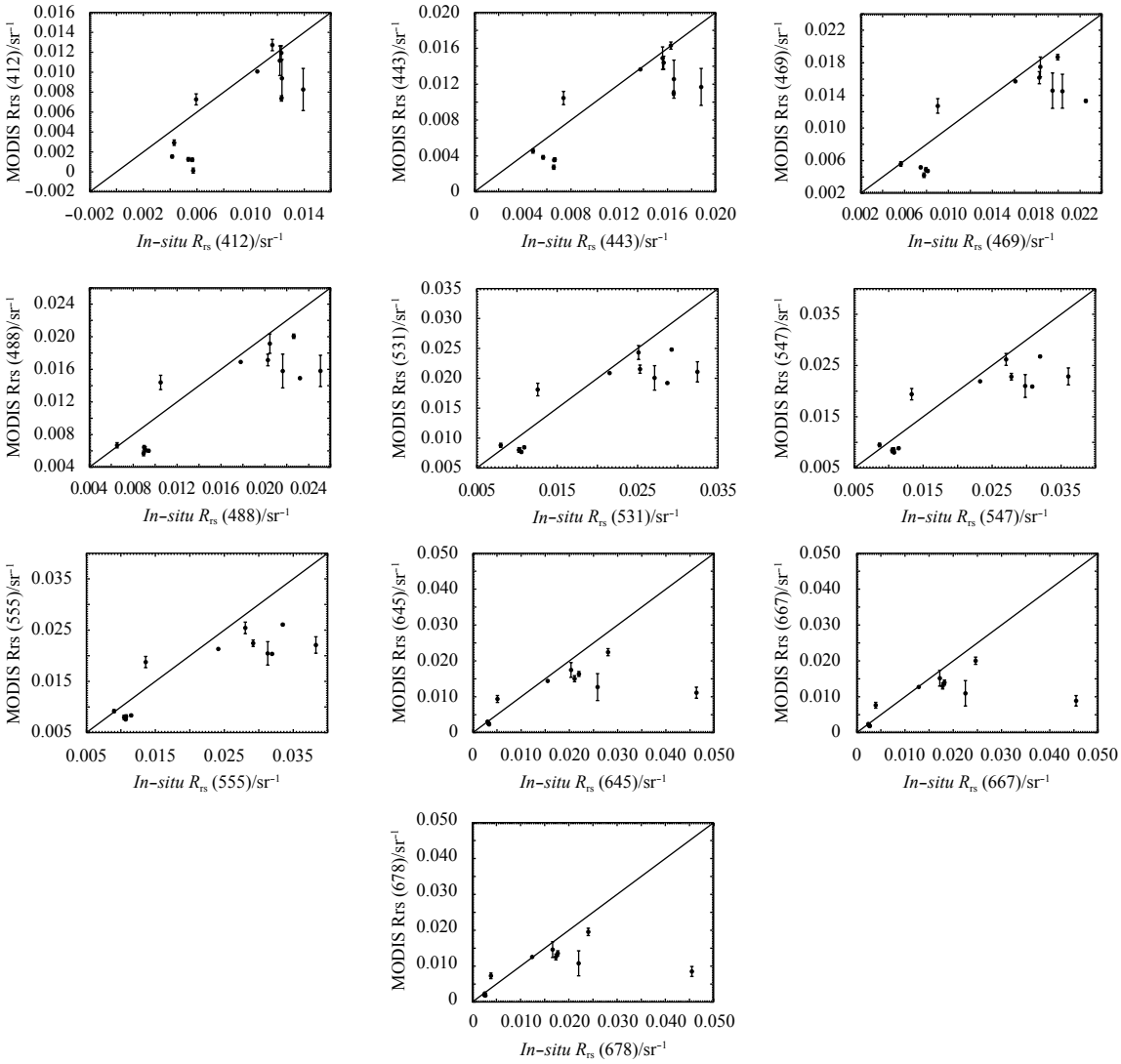

Fig. 6. Scatter plots of MODIS $R_{rs}(\lambda)$ versus *in-situ* $R_{rs}(\lambda)$ for the match-ups (N=13). The solid line represents a 1:1 line. The vertical error bars indicate the standard deviation across the 3×3 MODIS pixels.

hellemont and Ruddick, 2015; Wang and Shi, 2012; Werdell et al., 2010). Therefore, improving the performance of the atmospheric correction is still an important task in studying the coastal water.

At the same time, aerosol properties play an important role in the atmospheric correction. More than 50% of the resolved aerosol mass is contributed by anthropogenic sources. The anthropogenic contribution is influenced to a large extent by East Asian monsoons, with a significantly higher effect in spring and winter than in summer. This effect is associated with the change of prevailing wind directions from north/northwest (off the continent) to south/southeast (Wang et al., 2016). Furthermore, the aerosol optical depth (AOD) is an important parameter for the best use of satellite data. Previous research has shown that the MODIS-retrieved AODs are lower than those of *in-situ* data in turbid water. This is likely caused by the errors in aerosol model assumptions or overestimation of single scattering albedo (Prasad and Singh, 2007; He et al., 2010). The visible reflectance affects the aerosol properties, while the shortwave infrared or so-called near infrared reflectance affects the surface reflectance estimates in MODIS AOD retrieval, these effects could be a source of error for the MODIS-aqua data calibration (Kang et al., 2016; Xiong et al., 2007). If *in-situ* aerosol measurements synchronous with ocean colour data were available, it could provide the auxiliary aerosol information for the atmospheric correction. Additionally, this is helpful in providing a better understanding of the error source of $R_{rs}(\lambda)$.

4.2 *Development of regional ocean-colour algorithm*

Compared with the *in-situ* $R_{rs}(\lambda)$ (Table 1, Fig. 6), the MODIS-Aqua $R_{rs}(\lambda)$ was more accurate at 488 and 547 nm than it was at 412 and 443 nm. This indicates the possible errors in the atmospheric correction, affecting the blue bands (Tilstone et al., 2013). Of the 13 MODIS *in situ* Chl *a* match-ups obtained, OC3M uses $R_{rs}(488)/R_{rs}(547)$ which seems less affected by the atmospheric correction; however, compared with the *in situ* ratio, the determination coefficient R^2 was only 0.075. This is due to the tendency of MODIS-Aqua to under-estimate $R_{rs}(488)$ at high values (i.e., when Chl *a* is low). The use of the $R_{rs}(488)/R_{rs}(547)$ would result in a higher than expected ratio and therefore reflect higher Chl *a* values (Table 2).

We tested the red-NIR MODIS algorithm using our *in situ* dataset. Figure 9 depicts the relationship between Chl *a* and the

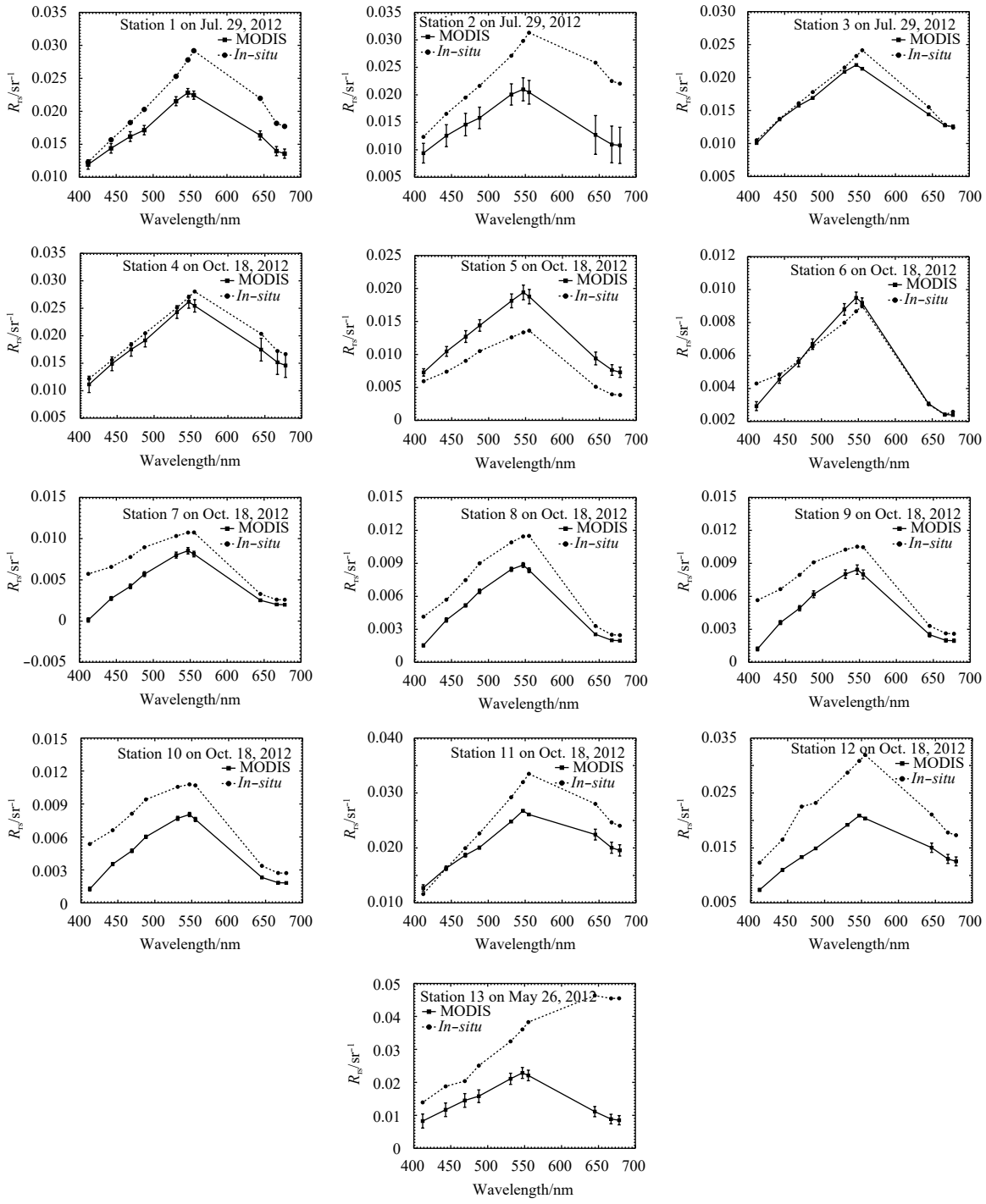

Fig. 7. Comparison between MODIS-derived and *in-situ* measured remote sensing reflectance R_{rs} (λ) for each of the 13 match-ups. The black circles connected by the dashed line represent *in-situ* data, while the squares linked with a solid line indicate MODIS products. The error bars represent the standard deviation of satellite retrievals and variability of in-situ measurements.

Table 2. Statistics of comparison between MODIS-derived products and *in-situ* measurements

Model name	APD/%	RMS	Ratio	SIQR	R^2	Slope	Intercept
MODIS-OC3M (Chl *a*)	132	2.49	2.72	0.73	0.05	0.076	4.37
Tang (SPM)	49	12.38	0.90	0.54	0.80	1.76	–1.98
Zhang (SPM)	33	5.85	0.88	0.25	0.86	0.51	2.25

Table 3. Statistics of comparison between the models-derived SPM and *in-situ* measurements

Model name	APD/%	RMS	Ratio	SIQR	R^2	Slope	Intercept
Original Tang	53	125.88	1.06	0.40	0.43	0.69	25.06
Adjusted Tang	49	113.82	1.03	0.37	0.45	0.57	24.84
Original Zhang	53	113.98	1.04	0.41	0.43	0.48	28.08
Adjusted Zhang	52	113.78	1.03	0.40	0.44	0.48	28.18

Table 4. SPM quantitative retrieval models

Model	Original model	Adjusted model
Tang	lgSPM=0.582+23.84×(R_{rs}(555)+R_{rs}(670))–0.485 3×(R_{rs}(490)/R_{rs}(555))	lgSPM=1.063+21.798×(R_{rs}(555)+R_{rs}(667))–1.04×(R_{rs}(488)/R_{rs}(555))
Zhang	lgSPM=0.631 1+22.215 8×(R_{rs}(555)+ R_{rs}(645))–0.523 9×(R_{rs}(488)/R_{rs}(555))	lgSPM=1.039+21.549×(R_{rs}(555)+ R_{rs}(645))–1.051×(R_{rs}(555)/R_{rs}(488))
Tassan	lgSPM=s_0+$s_1$lg(R_{rs}(555)+ R_{rs}(645))–$s_2$lg(R_{rs}(488)/R_{rs}(555))	lgSPM=3.199+1.628 l g (R_{rs}(555)+ R_{rs}(645))–3.003 l g (R_{rs}(488)/R_{rs}(555))
D'Sa	SPM=17.783(R_{rs}(670)/R_{rs}(555))$^{1.11}$	SPM=96.448(R_{rs}(667)/R_{rs}(555))$^{2.86}$

Note: The adjusted model is obtained by means of least-square fit to the original model using the measured data; S_0, S_1,S_2 numerical constants obtained from fits to measurements of concentration of SPM in water column.

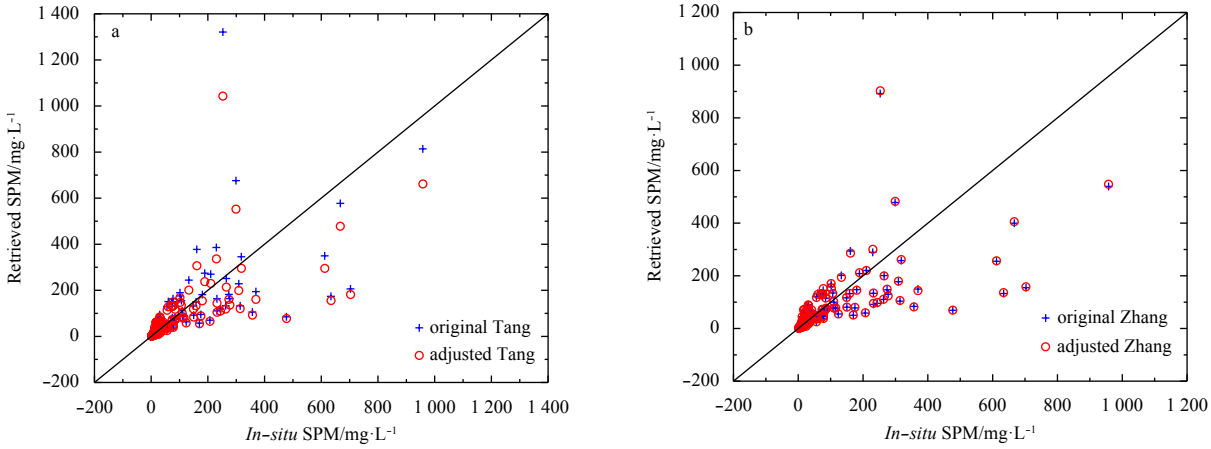

Fig. 8. Comparison between the models estimate SPM and *in-situ* measurements. a. Tang model; b. Zhang model

Table 5. Evaluation for the satellite-derived radiometric products with NIR-SWIR method

$R_{rs}(\lambda)$	APD/%	RMS	RPD/%	Ratio	SIQR	R^2	Slope
R_{rs}(412)/sr^{-1}	20	0.001 8	–16	0.802	0.067	0.885	0.851
R_{rs}(443)/sr^{-1}	16	0.002 5	–10	0.888	0.077	0.869	0.723
R_{rs}(469)/sr^{-1}	15	0.003 2	–8	0.900	0.072	0.822	0.667
R_{rs}(488)/sr^{-1}	17	0.003 8	–10	0.861	0.077	0.826	0.633
R_{rs}(531)/sr^{-1}	17	0.004 8	–8	0.901	0.086	0.844	0.623
R_{rs}(547)/sr^{-1}	18	0.005 6	–9	0.906	0.087	0.822	0.605
R_{rs}(555)/sr^{-1}	21	0.006 9	–14	0.862	0.083	0.818	0.559
R_{rs}(645)/sr^{-11}	27	0.010 7	–9	0.923	0.140	0.539	0.342
R_{rs}(667)/sr^{-1}	30	0.010 7	–5	0.994	0.161	0.437	0.285
R_{rs}(678)/sr^{-1}	29	0.010 8	–7	0.926	0.151	0.412	0.272
R_{rs}(555)+R_{rs}(645)/sr^{-1}	23	0.017 1	–14	0.880	0.079	0.714	0.451
R_{rs}(555)+R_{rs}(667)/sr^{-1}	23	0.016 9	–13	0.891	0.086	0.678	0.428
R_{rs}(488)/R_{rs}(555)	5	0.049 2	5	1.054	0.035	0.780	0.598
R_{rs}(555)/R_{rs}(667)	27	0.759 1	6	0.975	0.113	0.739	0.531
R_{rs}(443)/R_{rs}(555)	10	0.062 3	6	1.101	0.055	0.096	0.292
R_{rs}(412)/R_{rs}(488)	12	0.095 4	–5	0.971	0.071	0.000 04	0.010
R_{rs}(443)/R_{rs}(547)	7	0.049 5	–0.1	1.039	0.045	0.089	0.325
R_{rs}(488)/R_{rs}(547)	4	0.032 7	–1	0.988	0.029	0.718	0.571

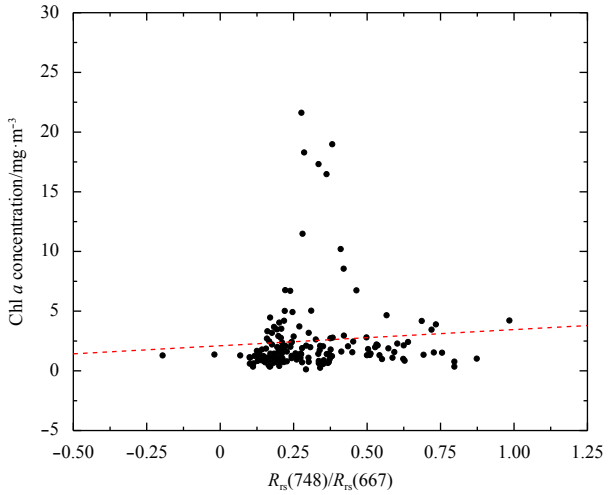

Fig. 9. Chl *a* conventration versus $R_{rs}(748)/R_{rs}(667)$.

$R_{rs}(748)/R_{rs}(667)$. However, the correlation coefficient is significantly lower (R^2=0.13) than those achieved by Gons et al. (2002, 2005) and others (Carswell et al., 2017; Yacobi et al., 2011; Gilerson et al., 2010; Moses et al., 2009). Besides the influence of the atmospheric correction, the reflectance spectra at the red and NIR bands were affected by possible variations in phytoplankton specific absorption coefficient, and perhaps were also influenced by the temporal variation of the water quality. Therefore, the NIR-Red models have substantial uncertainties when applied to multi-temporal data.

To improve the accuracy of the Chl *a* retrievals, Sun et al. (2010) and Shen et al. (2010) built a four-band algorithms and a SCI Chl *a* inversion method respectively for the turbid waters of Changjiang Estuary. The performance of these algorithms was compared with that of the MODIS-OC3M and MERIS-C2P. The accuracies yielded by the algorithms of Sun and Shen were better than those yielded by the MODIS and MERIS data. Thus, these two methods were also evaluated in our study, and the NIR-SWIR combined with the atmospheric correction was applied to the MODIS data (https://oceandata.sci.gsfc.nasa.gov/) (see Table 6 and Fig. 10a). Obviously, the accuracy was improved compared with the MODIS-derived Chl *a* value for the match-ups, especially when using the Sun algorithm. The APD was 31%, while the RMS was 1.527, which were higher than those in the study of Sun et al. Furthermore, the linear relationship between the *in-situ* and model estimated Chl *a* is still not obvious according to a low correlation coefficient R^2. We obtained results similar to that of Salem et al.(2017), who had assessed seven Chl *a* algorithms in Tokyo Bay, and found that two-band and four-band algorithms outperformed the other algorithms for the measured and simulated datasets, and the SCI algorithms showed the highest error for both datasets(Salem et al., 2017). For a Chl *a* concentration below 10 mg/m^3, the output of the algorithm is sensitive to variation in concentrations of total suspended solids and colored dissolved organic matter (Dall'Olmo and Gitelson, 2006). Thus, only single algorithm cannot provide outstanding accuracy for Chl *a* retrieval and multi-algorithms should be included and developed for different sea areas.

Compared with the Chl *a* Satellite retrieval algorithms, the performance of SPM regional models is better, but that still cannot meet the requirement for the SPM retrievals. Other popular models for coastal ocean, including the Tassan model (Tassan, 1993) and the D'Sa model (D'Sa et al., 2007), were also applied to the MODIS data which were processed by the NIR-SWIR atmospheric correction (see Table 4, Table 7 and Fig. 10b). Reasonable retrieval results were found by using the Tassan model in the range of approximately 1.7–26 g/m^3, which is similar to the SPM range for the match-ups. The RMS values calculated by using the Tassan model and the D'Sa model were 3.275 and 5.309, lower than those calculated by the Tang method and the Zhang method. The R^2 coefficients were 0.867 and 0.844, respectively. From our study, the modified Tassan coast model is more suitable for the SPM retrieval in the YS and ESC region. The average relative error was only 21%.

Therefore, large variability in the SPM and Chl *a* distributions exists along the coast, substitute algorithms are still needed, es-

Table 6. Statistics of comparison between derived and *in situ* measurements of Chl *a*

Model name	APD/%	RMS	Ratio	SIQR	R^2	Slope	Intercept
Sun	31	1.527	0.770	0.204	0.137	0.102	1.456
Shen	129	2.462	2.246	0.899	0.011	0.060	4.148

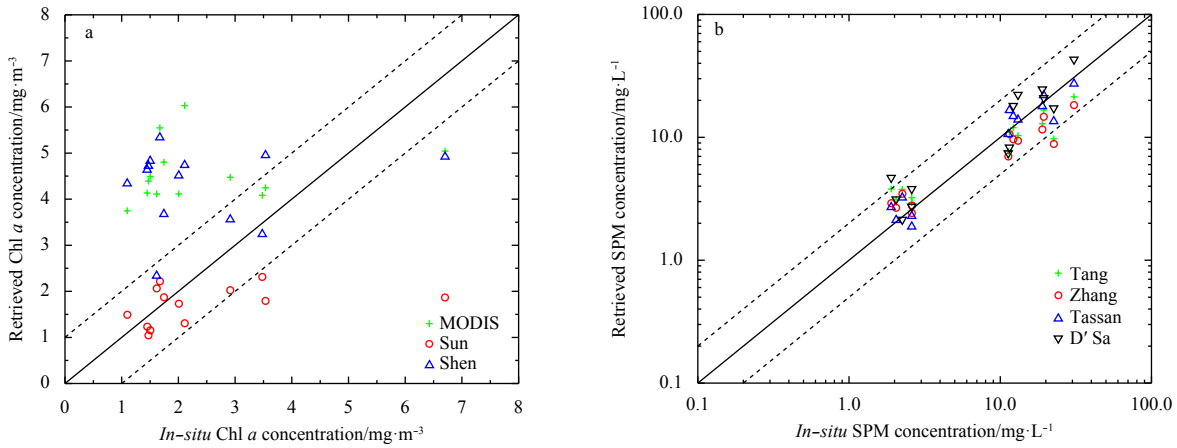

Fig. 10. Scatter plots of the derived value versus *in-situ* measurements. a. Chl *a* concentration and b. SPM concentration. The solid line is a 1:1 line. Dashed lines are 1:2 and 2:1 lines.

Table 7. Statistics of comparison between the costal models-derived value with newly processed R_{rs} and *in situ* measurements of SPM

	APD/%	RMS	Ratio	SIQR	R^2	Slope	Intercept
Tassan	21	3.275	1.003	0.165	0.867	0.846	1.605
Desa	41	5.309	1.294	0.265	0.844	1.191	–0.144
Tang	34	6.259	0.789	0.254	0.869	0.494	2.304
Zhang	32	5.966	0.790	0.224	0.864	0.508	2.121

pecially for those using the blue-green and NIR bands. A large number of match-ups between concurrent in situ and satellite data are also useful for Chl *a* and SPM estimation.

5 Conclusions

MODIS ocean-colour products along the YS and ECS were assessed based on a strict match-up analysis. The APDs of the MODIS $R_{rs}(\lambda)$ retrievals were in the range between 20% and 36%, and the highest uncertainty appeared at 412 nm. $R_{rs}(\lambda)$ at bands of 443 and 547 nm performed better. The band ratio of $R_{rs}(\lambda)$ at 488 to 547 nm showed high consistency with an APD of 7%. MDOIS Chl *a* product was found to be overestimated with a higher APD of 132%. Besides, two regional SPM retrieval algorithms were modified according to the in situ measurements and applied to the MODIS data, the derived SPM values underestimated the *in situ* ones, with the APDs of 49% and 33%, respectively.

By developing a better regional ocean-colour model, parameterized where possible to data from the YS and ECS, we were able to adjust the two ocean-colour empirical algorithms for Chl *a* estimation and used NIR-SWIR atmospheric correction to the MODIS data, and the accuracy was improved when compared with the MODIS-derived Chl *a* value. However, the linear correlation coefficients between in-situ and model estimated Chl *a* were still very small. In coastal waters enriched with nonalgal absorbing particles, the derivation of Chl *a* using the reflectance band ratio approach is subject to large errors owing to nonalgal materials that influence $R_{rs}(\lambda)$ but do not contribute to Chl *a*. Otherwise, the colored dissolved organic matter plays an important role for the water absorption and affects the reflectance band-ratios. Therefore, only single algorithm cannot provide outstanding accuracy for Chl *a* retrieval and that multi-algorithms should be included and developed for different sea area.

At the same time, the SPM modified algorithms were also applied to the MODIS data processed by NIR-SWIR atmospheric correction algorithm, and a comparison between the models estimated values and the measured SPM showed that the modified Tassan model obtained higher accuracy than other models along the YS and ECS, which utilizes the reflectance at bands of 488, 555, and 645 nm, the average relative error is only 21%. Given the limited match-up dataset and the potential influence of the aerosol properties on atmosphere correction, the model uncertainties also associated with the particle composition and size distribution, further research is required to develop additional algorithms for coastal water. Furthermore, a dedicated in situ data collection effort is highly needed for validating ocean-colour sensors.

Acknowledgements

This work was initiated when Lingling Jiang visited Plymouth Marine Laboratory funded by Dalian Maritime University and got many help from team members there for data processing. We thank all crew members on the cruises for their hard work in collecting and analyzing the *in situ* data. We also thank the NASA for their help with providing MODIS data.

References

Bailey W S, Werdell J P. 2006. A multi-sensor approach for the on-orbit validation of ocean color satellite data products. Remote Sensing of Environment, 102: 12–23, doi: 10.1016/j.rse.2006.01.015

Bailey S W, Franz B A, Werdell P J. 2010. Estimation of near-infrared water-leaving reflectance for satellite ocean color data processing. Optics Express, 18(7): 7521–7527, doi: 10.1364/OE.18.007521

Bian Changwei, Jiang Wensheng, Quan Qi, et al. 2013. Distributions of suspended sediment concentration in the Yellow Sea and the East China Sea based on field surveys during the four seasons of 2011. Journal of Marine Systems, 121–122(5): 24–35

Carder K L, Chen F R, Cannizzaro J P, et al. 2004. Performance of the MODIS semi-analytical ocean color algorithm for chlorophyll-*a*. Advances in Space Research, 33(7): 1152–1159, doi: 10.1016/S0273-1177(03)00365-X

Carswell T, Costa M, Young E, et al. 2017. Evaluation of MODIS-aqua atmospheric correction and chlorophyll products of western North American coastal waters based on 13 years of data. Remote Sensing, 9(10): 63–88

Chen Shuguo, Zhang Tinglu, Hu Lianbo. 2015. Evaluation of the NIR-SWIR atmospheric correction algorithm for MODIS-Aqua over the Eastern China Seas. International Journal of Remote Sensing, 35(11–12): 4239–4251

Cheng Chunmei, Wei Yuchun, Xu Jianjun, et al. 2013. Remote sensing estimation of Chlorophyll a and suspended sediment concentration in turbid water based on spectral separation. Optik, 124(24): 6815–6819, doi: 10.1016/j.ijleo.2013.05.078

Cui Tingwei, Zhang Jie, Groom S, et al. 2010. Validation of MERIS ocean-color products in the Bohai Sea: A case study for turbid coastal waters. Remote Sensing of Environment, 114(10): 2326–2336, doi: 10.1016/j.rse.2010.05.009

Cui Tingwei, Zhang Jie, Tang Junwu, et al. 2014. Assessment of satellite ocean color products of MERIS, MODIS and SeaWiFS along the East China Coast (in the Yellow Sea and East China Sea). ISPRS Journal of Photogrammetry and Remote Sensing, 87: 137–151, doi: 10.1016/j.isprsjprs.2013.10.013

Dall'Olmo G, Gitelson A, Rundquist D C, et al. 2005. Assessing the potential of SeaWiFS and MODIS for estimating chlorophyll concentration in turbid productive waters using red and near-infrared bands. Remote Sensing of Environment, 96(2): 176–187, doi: 10.1016/j.rse.2005.02.007

Dall'Olmo G, Gitelson A. 2006. Effect of bio-optical parameter variability and uncertainties in reflectance measurements on the remote estimation of chlorophyll-*a* concentration in turbid productive waters: Modeling results. Applied Optics, 45(15): 3577–3592, doi: 10.1364/AO.45.003577

Darecki M, Stramski D. 2004. An evaluation of MODIS and SeaWiFS bio-optical algorithms in the Baltic Sea. Remote Sensing of Environment, 89(3): 326–350, doi: 10.1016/j.rse.2003.10.012

Doxaran D, Cherukuru N, Lavender S J. 2006. Apparent and inherent optical properties of turbid estuarine waters: measurements, empirical quantification relationships, and modeling. Applied Optics, 45(10): 2310–2324, doi: 10.1364/AO.45.002310

D'Sa E J, Miller R L, McKee B A. 2007. Suspended particulate matter dynamics in coastal waters from ocean color: application to the northern Gulf of Mexico. Geophysical Research Letters, 34(23): L23611

Gao Xuelu, Song Jinming. 2005. Phytoplankton distributions and

their relationship with the environment in the Changjiang Estuary, China. Marine Pollution Bulletin, 50(3): 327–335, doi: 10.1016/j.marpolbul.2004.11.004

Gilerson A A, Gitelson A A, Zhou Jing, et al. 2010. Algorithms for remote estimation of chlorophyll-a in coastal and inland waters using red and near infrared bands. Optics Express, 18(23): 24109–24125, doi: 10.1364/OE.18.024109

Gitelson A A, Dall'Olmo G, Moses W, et al. 2008. A simple semi-analytical model for remote estimation of chlorophyll-*a* in turbid waters: Validation. Remote Sensing of Environment, 112(9): 3582–3593, doi: 10.1016/j.rse.2008.04.015

Gitelson A, Schalles J F, Hladik C M. 2007. Remote chlorophyll-a retrieval in turbid, productive estuaries: Chesapeake Bay case study. Remote Sensing of Environment, 109(4): 464–472, doi: 10.1016/j.rse.2007.01.016

Gons H J, Rijkeboer M, Ruddick K G. 2002. A chlorophyll-retrieval algorithm for satellite imagery (medium resolution imaging spectrometer) of inland and coastal waters. Journal of Plankton Research, 24(9): 947–951, doi: 10.1093/plankt/24.9.947

Gons H J, Rijkeboer M, Ruddick K G. 2005. Effect of a waveband shift on chlorophyll retrieval from MERIS imagery of inland and coastal waters. Journal of Plankton Research, 27(1): 125–127

Han L, Rundquist D C, Liu L L, et al. 1994. The spectral responses of algal chlorophyll in water with varying levels of suspended sediment. International Journal of Remote Sensing, 15(18): 3707–3718, doi: 10.1080/01431169408954353

He Qianshan, Li Chengcai, Tang Xu, et al. 2010. Validation of MODIS derived aerosol optical depth over the Yangtze River Delta in China. Remote Sensing of Environment, 114(8): 1649–1661, doi: 10.1016/j.rse.2010.02.015

Kang Na, Kumar K R, Yu Xingna, et al. 2016. Column-integrated aerosol optical properties and direct radiative forcing over the urban-industrial megacity Nanjing in the Yangtze River Delta, China. Environmental Science and Pollution Research, 23(17): 17532–17552, doi: 10.1007/s11356-016-6953-1

Knaeps E, Dogliotti A I, Raymaekers D, et al. 2012. *In situ* evidence of non-zero reflectance in the OLCI 1020 nm band for a turbid estuary. Remote Sensing of Environment, 120: 133–144, doi: 10.1016/j.rse.2011.07.025

Kuchinke C P, Gordon H R, Harding L W Jr, et al. 2009. Spectral optimization for constituent retrieval in Case 2 waters II: validation study in the Chesapeake Bay. Remote Sensing of Environment, 113(3): 610–621, doi: 10.1016/j.rse.2008.11.002

Lee Z, Carder K L, Steward R G, et al. 1996. Protocols for measurement of remote sensing reflectance from clear to turbid waters. Presented at SeaWiFS Workshop. Halifax

Li Shuangzhao, Yuan Dekui, Wang Xue. 2017. Improvement of SWIR atmospheric correction algorithm for case II water. Acta Scientiae Circumstantiae (in Chinese), 37(1): 104–111

Menon H B, Lotliker A A, Moorthy K K, et al. 2006. Variability of remote sensing reflectance and implications for optical remote sensing—a study along the eastern and northeastern waters of Arabian Sea. Geophysical Research Letters, 33(15): L15602, doi: 10.1029/2006GL026026

Mobley C D. 1999. Estimation of the remote-sensing reflectance from above-surface measurements. Applied Optics, 38(36): 7442–7455, doi: 10.1364/AO.38.007442

Moses W J, Gitelson A A, Berdnikov S, et al. 2009. Estimation of chlorophyll-a concentration in case II waters using MODIS and MERIS data-successes and challenges. Environmental Research Letters, 4(4): 045005, doi: 10.1088/1748-9326/4/4/045005

Mueller J L, Fargion G S, McClain C R. 2003. Ocean optics protocols for Satellite Ocean color sensor validation, revision 4, volume VI: Special topics in ocean optics protocols and appendices. Greenbelt, Maryland: Aeronautics and Space Administration of USA

Prasad A K, Singh R P. 2007. Comparison of MISR-MODIS aerosol optical depth over the Indo-Gangetic basin during the winter and summer seasons (2000–2005). Remote Sensing of Environment, 107(1–2): 109–119, doi: 10.1016/j.rse.2006.09.026

Salem S I, Higa H, Kim H, et al. 2017. Assessment of Chlorophyll-*a* algorithms considering different trophic statuses and optimal bands. Sensors, 17(8): 1746, doi: 10.3390/s17081746

Shen Fang, Zhou Yunxuan, Li Daoji, et al. 2010. Medium resolution imaging spectrometer (MERIS) estimation of chlorophyll-a concentration in the turbid sediment-laden waters of the Changjiang (Yangtze) Estuary. International Journal of Remote Sensing, 31(17–18): 4635–4650, doi: 10.1080/01431161.2010.485216

Shi Wei, Wang Menghua. 2014. Ocean reflectance spectra at the red, near-infrared, and shortwave infrared from highly turbid waters: A study in the Bohai Sea, Yellow Sea, and East China Sea. Limnology and Oceanography, 59(2): 427–444, doi: 10.4319/lo.2014.59.2.0427

Sun Ling, Guo Maohua, Wang Xiaomei. 2010. Ocean color products retrieval and validation around China coast with MODIS. Acta Oceanologica Sinica, 29(4): 21–27, doi: 10.1007/s13131-010-0047-6

Tang Junwu, Tian Guoliang, Wang Xiaoyong, et al. 2004. The methods of water spectra measurement and analysis I: Above-water method. Journal of Remote Sensing (in Chinese), 8(1): 37–44

Tassan S. 1993. An improved in-water algorithm for the determination of chlorophyll and suspended sediment concentration from Thematic Mapper data in coastal waters. International Journal of Remote Sensing, 14(6): 1221–1229, doi: 10.1080/01431169308904406

Tilstone G H, Lotliker A A, Miller P I, et al. 2013. Assessment of MODIS-Aqua chlorophyll-*a* algorithms in coastal and shelf waters of the eastern Arabian Sea. Continental Shelf Research, 65: 14–26, doi: 10.1016/j.csr.2013.06.003

Vanhellemont Q, Ruddick K G. 2015. Advantages of high quality SWIR bands for ocean colour processing: Examples from Landsat-8. Remote Sensing of Environment, 161: 89–106, doi: 10.1016/j.rse.2015.02.007

Wang Menghua, Shi Wei. 2007. The NIR-SWIR combined atmospheric correction approach for MODIS ocean color data processing. Optics Express, 15(24): 15722–15733, doi: 10.1364/OE.15.015722

Wang Menghua, Son S, Shi Wei. 2009. Evaluation of MODIS SWIR and NIR-SWIR atmospheric correction algorithms using SeaBASS data. Remote Sensing of Environment, 113(3): 635–644, doi: 10.1016/j.rse.2008.11.005

Wang Menghua, Shi Wei. 2012. Sensor noise effects of the SWIR bands on MODIS-derived ocean color products. IEEE Transactions on Geoscience and Remote Sensing, 50(9): 3280–3292, doi: 10.1109/TGRS.2012.2183376

Wang Lin, Zhao Dongzhi, Yang Jianhong, et al. 2012. Retrieval of total suspended matter from MODIS 250 m imagery in the Bohai Sea of China. Journal of Oceanography, 68(5): 719–725, doi: 10.1007/s10872-012-0129-5

Wang Fujiang, Chen Ying, Meng Xi, et al. 2016. The contribution of anthropogenic sources to the aerosols over East China Sea. Atmospheric Environment, 127: 22–33, doi: 10.1016/j.atmosenv.2015.12.002

Werdell P J, Franz B A, Bailey S W. 2010. Evaluation of shortwave infrared atmospheric correction for ocean color remote sensing of Chesapeake Bay. Remote Sensing of Environment, 114(10): 2238–2247, doi: 10.1016/j.rse.2010.04.027

Xiao Yanfang, Zhang Jie, Cui Tingwei, et al. 2018. A new merged dataset of global ocean chlorophyll *a* concentration with higher spatial and temporal coverage. Acta Oceanologica Sinica, 37(7): 118–130, doi: 10.1007/s13131-018-1249-6

Xiong Xiaoxiong, Sun Junqiang, Barnes W, et al. 2007. Multiyear on-orbit calibration and performance of Terra MODIS reflective solar bands. IEEE Transactions on Geoscience and Remote Sensing, 45(4): 879–889, doi: 10.1109/TGRS.2006.890567

Yacobi Y Z, Moses W J, Kaganovsky S, et al. 2011. NIR-red reflectance-based algorithms for chlorophyll-*a* estimation in mesotrophic inland and coastal waters: Lake Kinneret case study. Water Research, 45(7): 2428–2436, doi: 10.1016/j.watres.2011.02.002

Zhang Minwei, Tang Junwu, Dong Qing, et al. 2010. Retrieval of total suspended matter concentration in the Yellow and East China Seas from MODIS imagery. Remote Sensing of Environment, 114(2): 392–403, doi: 10.1016/j.rse.2009.09.016

Zibordi G, Berthon J F, Mélin F, et al. 2009. Validation of satellite ocean color primary products at optically complex coastal sites: Northern Adriatic Sea, Northern Baltic Proper and Gulf of Finland. Remote Sensing of Environment, 113(12): 2574–2591, doi: 10.1016/j.rse.2009.07.013

Zibordi G, Mélin F, Berthon J F. 2006. Comparison of SeaWiFS, MODIS and MERIS radiometric products at a coastal site. Geophysical Research Letters, 33(6): L06617